PHYSICAL REVIEW B **78**, 035429 (2008)

Diffusion piloted ordering in codeposited CoPt epitaxial layers: Experiment and quenched molecular dynamics simulations

O. Ersen, C. Goyhenex, and V. Pierron-Bohnes

Institut de Physique et Chimie des Matériaux de Strasbourg UMR 7504 CNRS-Université Louis Pasteur, 23 rue du Lœss, BP 43, F-67034 Strasbourg Cedex 2, France

(Received 26 October 2007; revised manuscript received 30 May 2008; published 16 July 2008)

This paper presents quenched molecular dynamics simulations of the vacancy behavior near the surface of an ordered CoPt alloy. The formation, migration, and activation energies are deduced for the different atoms (Co and Pt), moving in and between the different planes parallel to the surface. The migration of an adatom at the surface is also studied. The alloy surface is preferentially a Pt plane. There are typically two planes where the migration and formation energies are different from the bulk. The anisotropy of the structure involves an anisotropy of the diffusion. The values of the energies obtained for the different processes are used to understand the chemical ordering in CoPt(001) thin films grown at different temperatures. These films present indeed a concentration modulation along the growth direction with 2 temperature ranges. We analyze this behavior in terms of chemical ordering using a classical phenomenological diffusion law with the values of the energies deduced by quenched molecular dynamics.

DOI: 10.1103/PhysRevB.78.035429 PACS number(s): 61.05.cp, 66.30.Ny, 66.30.Pa, 68.35.Fx

I. INTRODUCTION

In the last decade, the growing interest for low dimension systems has implied a tremendous increase of the research on epitaxied layers. During the growth process of these systems, the proximity of the surface and the dynamical aspects make the prediction of the final state much more complicated than in the classical preparation methods.

To understand these phenomena, many aspects have to be taken into account: whereas in bulk single crystals the surface effects can be neglected, in layers grown by molecular epitaxy they are of importance. Bulk and surface are in competition both for interatomic interactions and diffusion. In the case of an alloy growth, the surface interactions can induce in the vicinity of the surface an order different from the order in the bulk for the same alloy.[1] A surface segregation of one component can also appear without any segregation tendency in the bulk system. For example, when the atomic size of the two species is very different, the minority atoms tend to segregate on the surface in order to relax the strains around it.[2] At the equiatomic stoichiometry, the larger atom will present a segregation tendency. A difference in surface energy can also induce a segregation of the element with the lower surface energy.

The kinetics phenomena are very sensitive to temperature. In intermetallics, the diffusion processes, necessary to change their order state, are based on the migration of vacancies[3] and the most important parameters are the migration and formation energies of vacancies which are very sensitive to the proximity of a surface. On or near a surface, the migration is strongly enhanced due to the abundance of vacancies in the surface plane and to the easier migration of adatoms and vacancies in the surface planes. Therefore, the equilibrium state of the chemical long-range order (CLRO) can be reached at lower temperature near a surface than in the bulk.

At the CoPt stoichiometry, the ordered alloys have the $L1_0$ structure (Fig. 1) that can be described as a stacking of pure Co and pure Pt (001) planes.[4] This phase is strongly anisotropic, which induces interesting physical properties (high magnetic anisotropy, shape memory). The atomic mobility in this ordered phase is also expected to be anisotropic and first simulation results of the migration inside the bulk have confirmed this atomic migration anisotropy.[5] In this paper, we present some quenched molecular dynamics (QMD) simulations of the migration of vacancies and adatoms on and near to the pure (001) surface of this phase in CoPt alloys.

After a short presentation of the calculation method, we calculate the following parameters: amount of relaxation for the two possible terminations, formation and migration energies of a vacancy within the different planes, migration energies of a vacancy between the different planes, and formation and migration energies of adatoms on the different surfaces.

In the discussion, the order of magnitude of the energies obtained through QMD are used to explain the CLRO variation in CoPt(001) alloy thin films deposited in epitaxy onto a

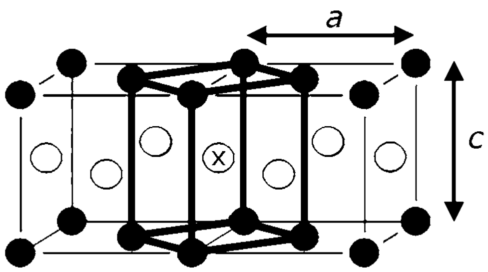

FIG. 1. Nearly face-centered-cubic cells generally used to describe the $L1_0$ structure ($c/a \approx 1$, thin lines). All lattice parameters and directions are given for this system in the text. The Bravais lattice is in fact a simple tetragonal structure (thick lines) with a Co atom at each edge and a unique Pt at the center (with a cross). The Bravais lattice is the unit cell that we have used to describe the slices as the atoms are placed on a simple square lattice in the (001) planes.

Pt(001) surface at different growth temperatures.[6] We propose a thermoactivated model to describe the chemical order variation as a function of growth temperature.

II. QUENCHED MOLECULAR DYNAMICS IN THE SECOND MOMENT APPROXIMATION OF THE TIGHT-BINDING METHOD IN $L1_0$ COPT

Quenched molecular dynamics is a standard relaxation procedure that allows the determination of the equilibrium structure of a system, at $T=0$ K, by integrating the equation of motion of its constituent atoms.[7] The quenching procedure consists in canceling the velocity of an atom when its projection on the force applied to this atom becomes negative. The calculation of the force $\vec{F}_i(t)$ on the atom at site i requires the knowledge of the energy E_i of each atom at site i. In the tight-binding formalism,[8] this energy is written as the sum of two terms: an attractive band energy E_i^b and a repulsive pair interaction E_i^r. The band term is obtained by integrating the local density of states up to the Fermi level,[8] which gives rise to the many-body character of the potentials necessary to account for surface relaxations and reconstructions.[9] When replacing the realistic density of states by a schematic density having the same second moment, i.e., the same full width at half maximum (*second-moment approximation*[10]), one obtains:

$$E_i^b = -\left\{ \sum_{\substack{j, r_{ij}<r_c \\ I,J=Co,Pt}} P_i^I P_j^J \xi_{IJ}^2 \exp\left[-2q_{IJ}\left(\frac{r_{ij}}{r_0^{IJ}} - 1 \right) \right] \right\}^{1/2}. \tag{1}$$

where P_i^I is the occupation operator of sites i by atoms I: it equals 1 if i is occupied by an atom I and 0 otherwise.

The exponent q_{IJ} characterizes the distance dependence of the hopping integral between atoms I and J at sites i and j. ξ_{IJ} is an effective hopping integral. r_0^{II} is the first-neighbor distance in I and $r_0^{IJ}=(r_0^{II}+r_0^{JJ})/2$. The interaction is neglected beyond a cutoff radius r_c.

The repulsive term E_i^r is described by a sum of Born-Mayer ion-ion repulsion energies:[11]

$$E_i^b = -\sum_{\substack{j, r_{ij}<r_c \\ I,J=Co,Pt}} P_i^I P_j^J A_{IJ} \exp\left[-p_{IJ}\left(\frac{r_{ij}}{r_0^{IJ}} - 1 \right) \right]. \tag{2}$$

The values of the parameters A, p, q, and ξ are taken from Ref. 12. More details on the QMD method can also be found in this paper and in the references therein. We have used this method to estimate the formation and migration energies of the different point defects contributing to the atomic mobility in these alloys and their sensitivity to a surface proximity.

A. Lattice parameter and defect formation energies in the bulk

The first step of the calculation was to obtain the lattice parameters of the bulk which corresponds to the considered (ξ, A, p, q) parameters. We defined in fct CoPt a three-dimensional cell with $10\times10\times30$ tetragonal unit cells with edges along $[110]$, $[1\bar{1}0]$, and $[001]$ of the underlying nearly face-centered-cubic phase (Fig. 1), respectively.

Periodic boundary conditions were used in all three directions. The total energy was minimized as a function of both a and c lattice parameters of the underlying face-centered-cubic lattice. The obtained optimal values are $a=0.39023$ nm and $c=0.351545$ nm for the slightly deformed cubic cell with a cohesion energy $\epsilon_0=5.36$ eV/atom. The latter value is in good agreement with the expected cohesion energy of the CoPt phase, 5.33 eV, as deduced from Ref. 13. The tetragonalization ($c/a=0.90$) is obtained at $T=0$ K and thus slightly larger than the experimental value ($c/a=0.96$ measured at $T\approx1000$ K).[4]

To describe the formation of a vacancy in the bulk, we empty one atomic site and let all atoms relax. The total-energy change gives access to the raw formation energy[14] of the vacancy because the concentration is not conserved: $\epsilon_{V_{\mathrm{Pt}}}=7.40$ eV and $\epsilon_{V_{\mathrm{Co}}}=6.09$ eV, respectively.

To have access to the effective vacancy formation energies, we have calculated the energy change when a Co is replaced by a Pt (Pt antisite), $\epsilon_{\mathrm{Pt_{Co}}}=-1.03$ eV, and when a Pt is replaced by a Co (Co antisite), $\epsilon_{\mathrm{Co_{Pt}}}=1.615$ eV. The true vacancy formation energies are then given by:[14]

$$E_F^{V_{\mathrm{Pt}}} = \epsilon_{V_{\mathrm{Pt}}} + \epsilon_0 + (\epsilon_{\mathrm{Pt_{Co}}} - \epsilon_{\mathrm{Co_{Pt}}})/4 = 1.39\ \mathrm{eV} \tag{3}$$

and

$$E_F^{V_{\mathrm{Co}}} = \epsilon_{V_{\mathrm{Co}}} + \epsilon_0 - (\epsilon_{\mathrm{Pt_{Co}}} - \epsilon_{\mathrm{Co_{Pt}}})/4 = 1.38\ \mathrm{eV}. \tag{4}$$

For the antisites, the effective formation energy is

$$E_F^{\mathrm{Pt_{Co}}} = E_F^{\mathrm{Co_{Pt}}} = (\epsilon_{\mathrm{Pt_{Co}}} + \epsilon_{\mathrm{Co_{Pt}}})/2 = 0.29\ \mathrm{eV}. \tag{5}$$

We have also calculated the formation energy of a pair of noninteracting Co,Pt vacancies. We get 2.76 eV, i.e., 1.38 eV per vacancy. When the two vacancies are formed on nearest-neighbor sites, the formation energy of the bivacancy is 2.36 eV. The difference (0.40 eV) corresponds to an energy diminution caused by the coupling between the two types of vacancies.

B. Vacancy formation energies near the surface

In all the following simulations, we have used similar cells with 30 planes along z (noted $n=0\ldots29$ with $n=29$ at the surface). Lateral periodic boundary conditions are applied in the x and y directions and the atomic positions are always initialized at the bulk positions. Before introducing any vacancy into the slab, we have calculated the surface energies and checked the effect of relaxation near the surface since relaxation is expected to play some role in the energetics of further vacancy formation and migration.

To ensure a bulklike configuration of the lowest atoms of the slice (to have a single surface), the atomic positions were fixed in the first four planes ($n=0\ldots3$). The total energy was calculated by summing E_i on $n=2\ldots29$ planes to ensure a complete second-neighbor shell for all relaxing atoms. We considered either Pt or Co terminated slabs. The energy per atom in the surface equals 0.785 eV/atom for a Co surface and 0.500 eV/atom for a Pt surface. The stability of the Pt

TABLE I. Formation ($E^{V_I}_{F,n}$), migration ($E^{V_I}_{M,n}$), and activation ($E^{V_I}_{A,n}$) energies of I vacancies within the n^{th} plane, and $E^{V_I}_{A,n,n+1}$, the activation energy for V_I migration from n^{th} surface-parallel plane to $n+1^{\text{th}}$ plane. The surface corresponds to $n=29$. The left set corresponds to the case of a Co surface, the right set to a Pt surface. All energies are in eV.

n	I	$E^{V_I}_{F,n}$	$E^{V_I}_{M,n}$	$E^{V_I}_{A,n}$	$E^{V_{\text{Co}}}_{A,n,n+1}$	$E^{V_{\text{Pt}}}_{A,n,n+1}$	I	$E^{V_I}_{F,n}$	$E^{V_I}_{M,n}$	$E^{V_I}_{A,n}$	$E^{V_{\text{Co}}}_{A,n,n+1}$	$E^{V_{\text{Pt}}}_{A,n,n+1}$
22	Pt	1:376	1.277	2.665	2.460	2.172	Co	1.393	1.294	2.675	2.462	2.182
23	Co	1.384	1.291	2.664	2.454	2.174	Pt	1.384	1.274	2.670	2.467	2.179
24	Pt	1.375	1.270	2.658	2.460	2.171	Co	1.393	1.291	2.672	2.459	2.182
25	Co	1.384	1.289	2.661	2.453	2.172	Pt	1.383	1.269	2.664	2.465	2.177
26	Pt	1.373	1.253	2.637	2.453	2.166	Co	1.390	1.273	2.651	2.454	2.176
27	Co	1.364	1.214	2.567	2.432	2.154	Pt	1.362	1.242	2.615	2.434	2.157
28	Pt	1.674	1.046	2.733	2.567	2.364	Co	1.575	1.172	2.735	2.503	2.242
29	Co	0.390	0.796	1.174	1.785	1.739	Pt	0.523	1.011	1.546	1.845	1.543

occupied surface compared to the Co surface in CoPt(001) is in good agreement with the experimental results.[1] Without relaxation, these energies are only 3–4 percents higher. Cutting bonds has the highest energy cost for both surfaces.

A slice of 30 planes is thick enough to avoid any relaxation in the $n=2$ to 10 planes. The planes remain flat and parallel to the bulk planes. As expected for surfaces of transition metals, an inward relaxation is obtained for the first plane.[9] For a Pt (Co) surface layer, the distance between the surface plane and the subsurface plane is 4% (5.5%) smaller than the distance of (001) planes in the bulk. A much smaller but noticeable relaxation is observed for the eight subsurface planes (from 0.15 to 0.05%).

To describe the formation of a vacancy in the plane n, we empty one atomic site in plane n and let all atoms relax except the $n=0$ to 4 planes. The total-energy change gives access to the raw formation energy[14] of the vacancy in plane n. The effective vacancy formation energy $E_{F,n}$ is calculated using the same relation as in the bulk [Eqs. (4) and (5)]. We find that the Pt and Co vacancy formation is not dependent on the distance to the surface and on the chemical nature of the surface plane up to the $n=27$ plane. In the surface and subsurface only, the values are different (Table I): the energy cost is lower in the surface plane ($\Delta E=-0.97$ eV for Co and -0.84 eV for Pt) and slightly higher in the subsurface plane ($\Delta E=+0.18$ eV for Co and $+0.31$ eV for Pt).

C. Migration energies of a vacancy within the different planes

The order parameter only changes when an atom migrates from a (001) plane to another and not when it migrates within a plane parallel to the surface. However, both phenomena must be considered to describe the ordering during codeposition as the atoms have to diffuse on the surface to find their final position. Moreover, some vacancies are trapped inside the sample and diffuse before being annihilated on the surface.

To describe the migration of a vacancy toward an atomic position in the plane n, we emptied one atomic site in plane n and let the next atom in the x direction move toward this site. The migrating atom was strained to move only in the plane perpendicular to its trajectory for all intermediate positions (constant-x plane). The total energy was minimized at each step with this strain. $E_{\text{total}}(x)$ presents two equal minima at $E_{\text{vac},n}$ when the atom is at both atomic positions.

The energy at these positions gives access to the raw formation energy of the vacancy in this plane. Between these two positions, the atom has to cross a saddle point with an energy maximum, related to the migration energy of the vacancy: $E_{M,n}=E_{\text{max}}-E_{\text{vac},n}$. The results are summarized in Table I. We find very similar values of the migration energy for the Co and Pt vacancies (within 0.03 eV), except in the three first planes at the surface. Surprisingly, the migration energy of a Pt atom is only significantly larger than the migration energy of a cobalt atom in the surface plane and in the sub-subsurface plane ($n=29$ and $n=27$, see right set of Table I). It is smaller in the subsurface plane ($n=28$, see left set of Table I). The migration energy of the vacancy is equal to 1.26–1.29 eV for both vacancies in all planes except in the four surface planes where it decreases progressively. The lower value is 0.80 eV for a Co vacancy in the surface plane.

Taking into account the effective formation energies, the total activation energy for the vacancy migration process is thus equal to 2.65 ± 0.10 eV in all planes and 1.55 eV for the vacancies at the surface if we consider the Pt surface that is the most stable.

D. Migration energies of a vacancy between different planes

The order parameter changes when an atom migrates from a (001) plane to another. The migration between the planes parallel to the surface is thus the most interesting in this context. We have plotted the variation of the total energy as a function of the apparent z position of the vacancy for the migration of an nearest neighbor of the vacancy initially in the next or preceding plane. The fictive trajectory of the vacancy between the two planes is deduced from the trajectory of the jumping atom as the symmetric with respect to the middle point. The curves are shown on Fig. 2. In the case of the $L1_0$ phase, the migration of a Pt (Co) vacancy out of its initial Pt-pure (Co-pure) plane gives rise to the formation of a Pt (Co) antisite. For this reason, the energies of two successive minima are different by 0.23 eV (0.21 eV). The antisite formation energy near a vacancy is slightly smaller at the surface than in the bulk.

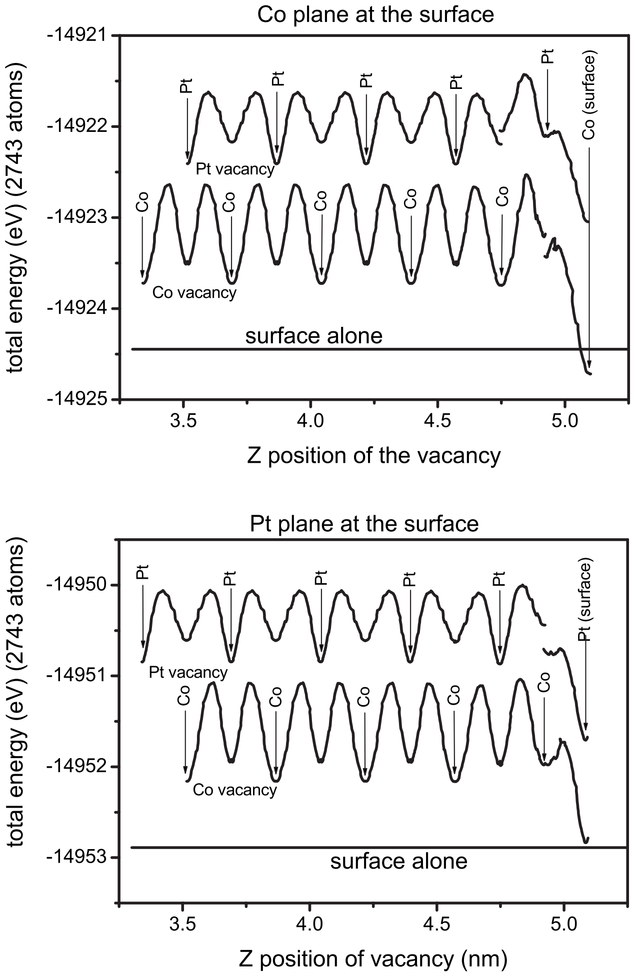

FIG. 2. Variation of the total energy when a vacancy migrates between two successive (001) planes for both the (a) Co and the (b) Pt surfaces. The labels near the arrows give the type of planes (pure Co or pure Pt planes). The curves have not been corrected for the concentration change for clarity reasons.

In the bulk, the migration energy with antisite formation corresponds to the barrier height from the deepest valley and equals 0.79 eV (1.08 eV) for a Pt (Co) vacancy. The migration energy with antisite annihilation equals 0.55 eV (0.87 eV). These migration energies are different when the two planes near to the surface are concerned. The smallest migration energy is obtained when the vacancy jumps from the subsurface (where its formation energy is the largest) to the surface plane (where its formation energy is the smallest). It equals 0.28 eV (0.05 eV) when the Co (Pt) vacancy jumps toward the Pt (Co) surface. The largest migration energy is similarly obtained when the vacancy jumps from surface plane to the subsurface plane. It equals 1.01 eV (1.41 eV) when the Pt (Co) surface vacancy jumps toward the subsurface.

The activation energy only depends on the saddle-point energy. The bulk values (2.2 eV for Pt vacancies and 2.45 eV for Co vacancies) are obtained except between the three surface planes (Table I).

E. Formation and migration energies of adatoms on the surface

We simulated the migration of the two types of adatom on the two types of surface. On the Pt surface, the trajectory of the adatom is more regular due to the rigidity of the Pt (001) plane, whereas some lateral movements are possible in the Co surface plane giving rise to correlated irregularities in trajectories and energy curves. The altitude of the adatom in the hollow site is slightly smaller than the distance of planes in the bulk (0.157 nm for Co and 0.174 nm for Pt instead of 0.176 nm).

The formation energy of an adatom is evaluated from the total energy at the minima of the curves and corrected for unlike numbers of Co and Pt atoms (using the same correction as for the vacancies). The lowest costs are to form Co adatoms on a Pt surface and Pt adatoms on a Co surface (see Table II), both continuing the growth of the $L1_0$ phase. The most unstable is Pt on a Pt surface that will be eliminated by a jump down in a vacancy in the surface plane to complete it. When moving on the surface, the adatom has a trajectory with a departure from the straight line in the z direction only: it moves between two positions in a hollow through a bridge between two atoms.

When an adatom jumps into a vacancy of the surface plane, the migration energy is mainly due to the horizontal jump necessary to attain the site nearest neighbor of the vacancy (unstable position of the atom). This jump has a migration energy similar to the jumps on the plane far from the vacancy. The reverse jump has a very high barrier energy due to the formation of both an adatom and a vacancy (Table II).

To summarize, the QMD simulations have shown that whereas the activation energy of the vacancies is higher than 2.5 eV in the bulk, near to the surface, some mechanisms have an activation energy smaller than 1 eV.

TABLE II. Formation ($E_F^{I/J}$), migration ($E_M^{I/J}$), and activation ($E_A^{I/J}$) energies (eV) of I adatom on a J surface. Migration energy of an I/J adatom into a vacancy in the surface plane ($E_M^{I/J\searrow I_J}$) and reverse ($E_M^{I_J\nearrow I/J}$).

I/J	$E_F^{I/J}$	$E_M^{I/J}$	$E_A^{I/J}$	$E_M^{I/J\searrow I_J}$	$E_M^{I_J\nearrow I/J}$
Pt/Co	0.683	1.095	1.778	1.090	2.170
Co/Co	0.540	0.904	1.444	0.940	1.870
Co/Pt	0.136	0.761	0.897	0.827	1.447
Pt/Pt	0.882	0.916	1.798	0.997	2.385

III. EXPERIMENTAL DETAILS

The values for the activation energies obtained by molecular dynamics simulations can be used to explain the chemical ordering in epitaxially grown CoPt thin films.

A. Sample preparation

The samples have been prepared by molecular beam epitaxy (MBE) with a 10^{-11} torr base pressure. The sample holder is in contact with a molybdenum wire furnace to reach different growth temperatures. Due to the heating in high vacuum, we expect some temperature fluctuations in time and in position on the sample holder (± 10 K).

The alloy thin layers have been prepared by codeposition at different growth temperatures (T_G). The CoPt(001) layers have been deposited at the equiatomic composition on a MgO(001) substrate with a Pt buffer layer deposited at 970 K. To prevent the samples from oxidation, they were covered by a 4 nm thick Ru cap layer deposited at 270 K. The concentrations had been optimized in previous series of samples using different flux ratios and were confirmed by *ex situ* EDX analysis. The sample thickness and composition were also verified by x-ray reflectometry. More details on the preparation conditions and optimization can be found elsewhere.[6]

The nominal thickness of the alloy films was generally 50 nm, which corresponds to a total deposition time of 3600 s, excepting the CoPt sample grown at T_G=780 K for which thickness and deposition time were the half (25 nm, 1800 s). To compensate the difference in the annealing time during the deposition, it has been annealed *ex situ* during 1800 s at 780 K. The average value of the CLRO parameter before and after annealing is comparable to that of the other samples. As a matter of fact, a 50 nm thick sample can be cut in mind into two 25 nm thick samples where the top sample is an as-grown sample and the bottom sample is equivalent to the same sample *ex situ* annealed at the growth temperature during the time necessary to grow a 25 nm thick sample.

B. Sample characterization

X-ray diffraction measurements were performed on a diffractometer equipped with the Co $K\alpha$ incident beam ($\lambda = 0.17889$ nm). $\theta/2\theta$ reflection scans and rocking curves in symmetrical geometry were collected. In particular, $\theta/2\theta$ x-ray diffraction (XRD) scans have allowed the determination of the lattice parameter along the growth axis, as well as the evidence of the chemical order along the growth axis.

We have shown in a previous paper[6] that the microstructure is related to the buffer layer quality, whereas the CLRO within the grains grown along a [001] direction mainly depends on the growth temperature.

In addition to the fundamental peaks characteristic of the buffer and alloy layers, the 001 and 003 superstructure peaks can be observed for the alloy layers, with amplitudes which depend on the growth temperature. No other superstructure peak was observed (100 and 010 peaks corresponding to in-plane concentration modulations for example), even by using a x-ray high-flux beam (synchrotron radiation). The diffracted intensities have been optimized versus the orientation of the sample around both axes in its plane so that the integrated intensities of the different peaks can be quantitatively measured and compared.

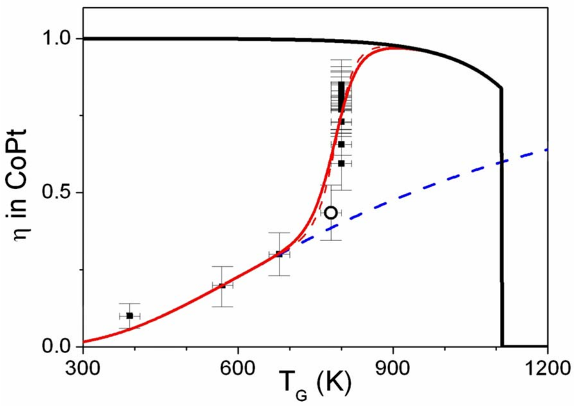

FIG. 3. (Color online) Temperature dependence of the CLRO parameter η in the CoPt(001) films. The dashed (blue online) thick line shows the surface contribution; the thin (red online) lines show the variation of η with the bulk contribution (2 eV: full, 2.5 eV: dashed). The thick black line is the variation of η in the bulk as calculated in the cluster-variation method (Ref. 20).

The Debye-Waller attenuation factors were measured on one sample (CoPt with T_G=780 K) on the W22 instrument of the LURE (Ref. 15) using a small wavelength in order to get high order diffraction peaks.[6] These values [$B_F = 0.0076(6)\text{nm}^2$ for the fundamental peaks and $B_S = 0.0156(20)\text{nm}^2$ for the superstructure peaks] were applied to the diffraction peak intensities of all samples.

C. Temperature variation of the chemical order parameter in CoPt

The $L1_0$ ordered structure of CoPt alloys at the equiatomic composition can be described as a stacking of pure Co and pure Pt (001) planes which define two sublattices α and β. In partially $L1_0$-ordered CoPt layers, the degree of chemical order is usually described by the CLRO parameter η defined as $\eta = |X_\alpha - X_\beta|$, where $X_{\alpha(\beta)}$ is the Co concentration on the $\alpha(\beta)$ sublattice. For all CoPt samples, the CLRO parameter was deduced independently from two intensity ratios between a superstructure and a fundamental peak, I_{001}/I_{002} and I_{003}/I_{004} after usual corrections and assuming the same values of the *D-W* factors for 001 and 003 superstructure peaks and 002 and 004 fundamental peaks, respectively. Both ratios give the same values of η within the error bars.

The growth temperature dependence of the chemical order parameter in the CoPt equiatomic system is shown in Fig. 3 in comparison with the calculated CLRO parameter in a bulk alloy at equilibrium.[20] The CLRO parameter variation in a bulk alloy (thick line on Fig. 3) is classical for a long-range order with a first-order transition: it equals 1 at low temperature, decreases progressively in a first stage, and falls down abruptly at the order-disorder transition that takes place at 1100 K in CoPt. In a bulk alloy quenched from an intermediate temperature and isochronally annealed at increasing temperature, the CLRO variation presents two stages: at low temperature, the CLRO is constant and when the atomic migration is possible, the curve joins progressively the equilibrium curve.[16] If the quench is made from very high temperature so that vacancies in sursaturation are trapped in the alloy, the LRO recovery takes place in three stages; between the two preceding stages appears a stage where the sursaturation vacancies contribute to the ordering before being annihilated.[16]

In the films, the variation with the growth temperature has similarities with this last case: after a plateau at very low temperature, the CLRO increases slowly in a first stage and very rapidly in a second stage. It has not been possible to observe in CoPt if the bulk value is attained at high temperature because the Pt buffer layer, necessary to obtain a flat surface and a good order state, prevents from annealing at high temperature due to the interdiffusion with the alloy layer. Note that an interdiffusion can only decrease the CLRO parameter because the maximum order parameter is obtained at the stoichiometry.

In the next paragraph, we briefly present the analysis of previous results in similar systems where the equilibrium bulk state is more easily attained and evidenced.

D. Temperature variation of the CLRO parameter in other systems: Co_3Pt and Co_3Ru

To further support the presence of two separated regimes as a function of the growth temperature, we can consider some results that were obtained by other authors in two similar systems, Co_3Pt and Co_3Ru.[17,18] In opposition to the CoPt system where the concentration modulation along the growth axis (CMAGA) creates in the thin layers a chemical order identical to the bulk equilibrium CLRO ($L1_0$ structure), in these systems, both orders are different. In the Co_3Pt system, the bulk equilibrium phase[4] is $L1_2$ (fcc above 600 K), whereas in the Co_3Ru system, the bulk equilibrium state is the disordered hexagonal compact phase (hcp). In the case of epitaxial layers, as the stable structure of pure cobalt is hcp, Co-rich alloys often grow in the hcp structure. Then, the CMAGA formed in the films is a hcp-DO_{19}-like structure (succession of Co-rich and Co-poor planes along [0001] in hcp) in both $Co_3Pt(0001)$ and $Co_3Ru(0001)$. This CMAGA order is evidenced in all cases by the appearance of a strong perpendicular anisotropy due to the strain induced by the concentration modulation and to the change of Pt-Co bond distribution. In $Co_3Pt(0001)$ and $Co_3Ru(0001)$, a 0001 superstructure peak appears. Its intensity gives access to the CLRO parameter associated with the CMAGA. In all cases, the bulk order is recovered when the CMAGA (quantified by the 0001 peak intensity) falls down to zero. In Co_3Ru and Co_3Pt, the 0001 superstructure peak disappear above 650 K showing that the disordered phase, the bulk equilibrium phase, is recovered.

IV. DISCUSSION

The experimental results have shown that in CoPt(001) where the CMAGA order is the same as the equilibrium chemical order the ordering takes place in two steps, whereas in the other systems where both orders are different, the metastable CMAGA order can be observed in a small temperature range between the low temperatures where the alloy is disordered and the high temperatures where the bulk equilibrium order is formed.

The quenched molecular dynamics simulations have shown that the activation energy of the vacancies is similar in all inner planes: 2.5–2.8 eV for both in-plane and between-planes migrations. The vacancies in the two surface planes and the adatoms have a different behavior. Their role is mostly important during the growth, because the atomic flux continuously creates surface vacancies and adatoms. The energy piloting the surface phenomena is thus the migration energy of these defects and not the sum of the formation and migration energies as for vacancies in the bulk. The order of magnitude of this migration energy spreads out between 0.1 and 1.5 eV for all surface processes considered in the previous part. Thus, we expect two distinct ranges in temperature: at lower growth temperature, the bulk migration is blocked and the final state will be the evidence of the surface process during the growth whereas at high temperature, this state will be changed due to bulk atomic migration in the bottom layers during the growth of the top layers.

A. Description of the ordering kinetics

Two different descriptions can be used to describe the kinetics of ordering depending on the predominant mechanism: either a homogeneous ordering, or the nucleation and growth of the ordered phase within the disordered one. As the order appears continuously at the surface without nucleation and afterwards varies in the following heat treatments, the kinetics of ordering can be described using the homogeneous ordering model.

Because of the proximity of the surface during the preparation, we propose here a thermally activated model that takes into account chemical ordering in two different ranges: the surface bilayer and the inside layers. The driving force of the surface ordering is predominantly the surface segregation[1] [leading to a bilayer-by-bilayer growth mode as clearly observed in FePd(001) thin layers[19]], whereas the driving force of the inside ordering is due to the bulk interactions (responsible of $L1_0$ chemical order in CoPt bulk samples). When the surface segregation and the bulk order are not compatible as in $Co_3Ru(0001)$ or $Co_3Pt(0001)$ films, the competition between both effects is evidenced, thanks to the mobility difference in both ranges[18] and gives rise to a maximum in $\eta(T_G)$. In the case of CoPt(001) layers, both are compatible and $\eta(T_G)$ has a variation with two steps.

To describe the chemical ordering in MBE grown layers, we can consider that the order parameter tends toward its equilibrium value in both surface and bulk ranges with a relaxation time given by Arrhenius laws.[4,16] The equations giving the evolutions of the order parameters as well as the relaxation times are presented in the Appendix. The variables are the pre-exponential factor for the relaxation time and the activation energies for atomic diffusion. We assume that the initial value of the order parameter is equal to 0 at the surface, whereas inside, it is given by the final value obtained at the surface after the deposition of a bilayer. To obtain the final value of the order parameter, we integrate over the total thickness of the layer, because each bilayer is annealed during the deposition time remaining after its deposit, which depends on its position in the sample. The evolution of the CLRO parameter inside the layer is similar to that in an *ex situ* annealing. In the latter process, all bilayers are annealed for the same duration. The parameters of the equation describing the CLRO evolution are those of bulk samples. The formalism developed in the Appendix is now applied to the different thin layers.

B. Application to the CoPt system

In the CoPt system, the equilibrium phase in bulk is the $L1_0$ phase[4] with three possible equivalent [100] crystallographic directions for the CLRO (the three variants). However, the MBE layers grown on a Pt(001) buffer layer present mainly only one variant, the variant with the chemical order along the growth direction[6] because this variant is the only variant compatible with the surface segregation during the growth and because it is favored by the strain due to the lattice misfit (lattice parameter larger in Pt).

Let us first consider the increase of the order parameter during the *ex situ* annealing of the particular sample deposited at 780 K to obtain information on the bulk diffusion parameters. Using the parameter values before $[\eta_{\text{initial}}=0.36(3)]$ and after $[\eta(1800\ \text{s},780\ \text{K})=0.51(6)]$ the *ex situ* annealing and the equilibrium bulk LRO parameter at this temperature[20] ($\eta_{B,\text{eq}}=0.993$), we get from Eq. (A3) of the Appendix: $\text{Ln}[\tau_B(780\ \text{K})]=9.0(7)\text{s}$.

Considering that the bulk activation energy in CoPt is within the interval 2–2.5 eV (QMD simulations and Ref. 4), we can evaluate the change of the CLRO in the first bilayer due to the annealing between its coverage by the second bilayer and the end of the film preparation. We find it smaller than one percent for the three lowest temperatures. Thus, at these temperatures, the evolution of the order parameter is only driven by the surface atomic mobility.

We have assumed that in this system, $\eta_{B,\text{eq}}\approx\eta_{S,\text{eq}}\approx 1$ below 600 K as shown by the theoretical variation (from cluster-variation method[20]). E_S, the activation energy of the surface diffusion, was estimated from the experimental points at 570 and 680 K and Eq. (A1) $[E_S=0.14(5)\text{eV}]$. The low E_S value shows that the kinetics is piloted by surface diffusion driven by a strong segregation tendency. η_S has been extrapolated at higher temperature [(blue online) thick dashed line on Fig. 3]. The departure of the point at 390 K can be explained by the thermal inertia of the sample holder, the true temperature on the sample may be higher than that given by the thermocouple.

The CLRO behavior on the whole temperature range is simulated with Eq. (A2) taking into account surface and bulk diffusions. The two (red online) thin lines in Fig. 3 correspond to $E_B=2$ (full) and 2.5 (dashed) eV (E_B is the activation energy of the bulk diffusion). The large fluctuations of the CLRO parameter observed around 800 K are explained by small temperature deviations (due to a relatively inhomogeneous temperature on the molybdenum block) amplified by the strong η increase when the bulk mobility becomes efficient.

The optimum preparation appears to be around 900 K; this temperature is high enough to ensure both surface and bulk mobility efficiencies and low enough to avoid the high-temperature decrease of chemical order in the bulk samples. Nevertheless, at such a high temperature, interdiffusion takes place at the interface with a buffer layer preventing in this case from using a Pt buffer. We then used a CoPt 10 nm buffer layer but could not get η values as high as in the bulk samples. The maximum value obtained without Pt buffer layer[6] is 0.75. This can be explained by the presence of numerous defects in the layers due to defects on the substrate surface. Indeed, monoatomic steps on the substrate induce antiphase boundaries in the ordered alloy film making the order parameter decrease.[19] As the metal surfaces are known to be smoother than oxide surfaces, the density of monoatomic steps is certainly lower on the surface of the Pt buffer layer. The average order measured by XRD in CoPt layers directly deposited onto MgO is thus expected to be lower than in CoPt layers deposited onto a Pt buffer layer. Moreover, disorder at the sub-boundaries between columns due to the epitaxial strains also diminishes the average CLRO.

A difference in CLRO parameter limit does not change significantly the bulk activation energy. It can partly explain that the pre-exponential factors ($\tau_{0B}=3.4\times 10^{-10}$ and 2.6×10^{-12} s, respectively, for $E_B=2$ and 2.5 eV) are larger than those obtained in bulk material:[4] 1.4×10^{-12} s for $E_B=2$ eV. The two curves (corresponding to $E_B=2$ and 2.5 eV) reproduce very well the dependence of the CLRO parameter as a function of the growth temperature.

C. Application to the Co_3Pt and Co_3Ru systems

The temperature dependences of the CMAGA in these systems can be interpreted as in the CoPt system, taking into account that the CMAGA order parameter equals zero at equilibrium according to the phase diagrams. The surface diffusion allows the formation of a partially ordered alloy with a CMAGA driven by surface segregation effect. When the temperature is low, the atomic diffusion is not efficient enough to exchange atoms (neither on the surface, nor in the bulk) and the atoms, randomly deposited by the atomic beams, remain randomly positioned on the crystal lattice. At medium temperatures, the surface diffusion is efficient and allows the ordering of the surface layers, whereas the bulk diffusion is not efficient. Therefore, the bilayers remain ordered after their coverage and a metastable ordered phase with a CMAGA can be observed. When the bulk diffusion becomes efficient, as the equilibrium phase inside the film is different of this metastable phase, the metastable CMAGA disappears except in the surface layer. The order parameter averaged on the whole thickness becomes 0.

The evolution of the order parameter in Co_3Pt and Co_3Ru samples can also be well reproduced using Eq. (A2) of the Appendix with the following values for the activation energies (Fig. 4): $E_B=2.5(1.0)\text{eV}$ and $E_S=0.39(6)\text{eV}$ in Co_3Pt and $E_B=2.5(2)\text{eV}$ and $E_S=1.0(2)\text{eV}$ in Co_3Ru. The differ-

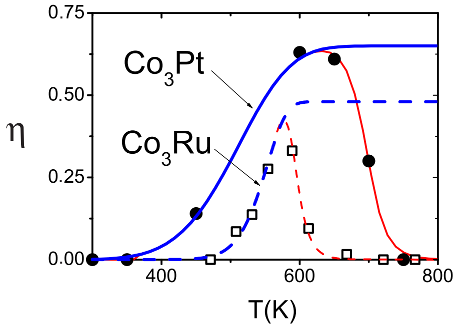

FIG. 4. (Color online) Temperature dependence of the CMAGA order parameter η in the $Co_3Pt(111)$ and $Co_3Ru(0001)$ films. The thick (blue online) line shows the surface contribution; the thin (red online) line show the bulk contribution. The full and dashed lines, circles and squares correspond, respectively, to the $Co_3Pt(0001)$ and $Co_3Ru(0001)$ films.

ence between the two energies in each system is responsible for the slope difference between the increasing and decreasing part of the curves. We get $\eta_{S,\mathrm{eq}}=0.5$ in Co_3Ru and 0.65 in Co_3Pt (the maximum values of η is 1). In both cases, the variation of the order parameter with the growth temperature is well reproduced.

V. CONCLUSION

In the CoPt system, we have observed and explained an ordering in two steps. At the lowest temperatures, the surface atomic migration forms the $L1_0$ phase with a low LRO parameter ($\eta=0.3$) due to the short duration of a bilayer growth. At higher temperatures, the ordering is continued by bulk atomic migration up to $\eta=0.85$.

The molecular dynamics simulations allow a better understanding of the surface atomic mobility which is responsible of the concentration modulation along the growth direction. Thanks to this effect, it is possible to grow thin films as single variants because the bulk order is initiated by the surface order. Indeed, if a disordered CoPt bulk sample is annealed, the three variants of the $L1_0$ phase are formed,[21] whereas a single-variant partially ordered layer remains single-variant when annealed.[22] This is of main importance to obtain samples with a macroscopic anisotropy as necessary for magnetic storage or shape memory applications.

APPENDIX: MODELING OF THE CLRO PARAMETER DEPENDENCE ON GROWTH TEMPERATURE

During the time necessary to deposit one bilayer (t_0), the order parameter within the surface bilayer (η_S) tends toward the maximum value at the surface $\eta_{S,\mathrm{eq}}$ with a relaxation time (τ_S) given by an Arrhenius law:

$$\eta_S(T_G) = \eta_{S,\mathrm{eq}} + (\eta_I - \eta_{S,\mathrm{eq}})\ e^{-t_0/\tau_S(T_G)}, \tag{A1}$$

with $\tau_S(T)=\tau_{0S}\ e^{E_S/k_BT}$, η_I the initial value of the surface order parameter, *a priori* equal to 0, k_B the Boltzmann constant, τ_{0S} the surface pre-exponential factor, and E_S the activation energy of the surface diffusion.

We have found using molecular dynamics that the activation energy is very similar in all inside layers. After the formation of N bilayers, during the deposition of next bilayers ($N+1, N+2, N+3\ldots$), the evolution of CLRO parameter in the N^{th} bilayer continues through bulk diffusion and the relaxation mechanism is similar to that of the order relaxation in intermetallics:[3] atomic mobility through bulk vacancy jumps. The bilayer evolves during t, the remaining deposition time that depends on the bilayer position in the sample ($t=t_1-t_0$ for the first deposited bilayer, with t_1 the total deposition time and t_0 the deposition time for one bilayer, and $t=0$ and t_0 for the last and penultimate deposited bilayers, respectively). The final order parameter is the averaged value over all bilayers, or equivalently over the deposition time t:

$$\begin{aligned}\eta_B(T_G) &= \frac{1}{t_1}\left[\int_0^{t_1-t_0}\{\eta_{B,\mathrm{eq}} + [\eta_S(T_G) - \eta_{B,\mathrm{eq}}]\ e^{-t/\tau_B(T_G)}\}dt \right.\\ &\qquad \left. + \ \eta_S(T_G)\ t_0\right]\\ &\approx \eta_{B,\mathrm{eq}} + [\eta_S(T_G) - \eta_{B,\mathrm{eq}}][1 - e^{-t_1/\tau_B(T_G)}]/[t_1/\tau_B(T_G)]\end{aligned} \tag{A2}$$

with $\tau_B(T)=\tau_{0B}\ e^{E_B/k_BT}$ and assuming that $t_0 \ll t_1$, which is a good approximation because t_1 and t_0 correspond, respectively, to the growth of 50 and 0.27 nm. $\eta_{B,\mathrm{eq}}$ is the equilibrium value of η in the bulk, τ_{0B} the bulk pre-exponential factor, and E_B the activation energy of the bulk diffusion.

During an *ex situ* annealing at temperature T_A, the evolution of the CLRO parameter is controlled by the bulk diffusion and can be written as:

$$\eta(t, T_A) = \eta_{B,\mathrm{eq}} + (\eta_{\mathrm{initial}} - \eta_{B,\mathrm{eq}})\ e^{-t/\tau_B(T_A)}. \tag{A3}$$

---

[1] M. C. Saint-Lager, R. Baudoing-Savois, M. De Santis, P. Dolle, and Y. Gauthier, Surf. Sci. **418**, 485 (1998); Y. Gauthier, R. Baudoing-Savois, J. M. Bugnard, W. Hebenstreit, M. Schmid, and P. Varga, *ibid.* **466**, 155 (2000).

[2] C. P. Flynn, Phys. Rev. Lett. **57**, 599 (1986).

[3] W. Petry, A. Heiming, C. Herzig, and J. Trampenau, Defect Diffus. Forum **75**, 211 (1991).

[4] C. Leroux, M. C. Cadeville, V. Pierron-Bohnes, G. Inden, and F. Hinz, J. Phys. F: Met. Phys. **18**, 2033 (1988).

[5] V. Pierron-Bohnes and T. Mehaddene, in *Alloys Physics: A Comprehensive Reference*, edited by W. Pfeiler (Wiley, Weinheim, Germany, 2007), p. 162.

[6] O. Ersen, V. Parasote, V. Pierron-Bohnes, M. C. Cadeville, and C. Ulhaq-Bouillet, J. Appl. Phys. **93**, 2987 (2003).

[7] C. H. Bennett, in *Diffusion in Solids, Recent Developments*, edited by A. S. Nowick and J. J. Burton (Academic, New York, 1975), p. 73.

[8] J. Friedel, in *The Physics of Metals*, edited by J. M. Ziman

(Cambridge University Press, Cambridge, 1969), p. 340.

[9] B. Legrand, M. Guillopé, J. S. Luo, and G. Tréglia, Vacuum **41**, 311 (1990).

[10] V. Rosato, M. Guillopé, and B. Legrand, Philos. Mag. A **59**, 321 (1989).

[11] F. Ducastelle, J. Phys. (Paris) **31**, 1055 (1970).

[12] C. Goyhenex, H. Bulou, J.-P. Deville, and G. Tréglia, Phys. Rev. B **60**, 2781 (1999).

[13] G. Rossi, R. Ferrando, and C. Mottet, Faraday Discuss. **138**, 193 (2008).

[14] Y. Mishin and Chr. Herzig, Acta Mater. **48**, 589 (2000).

[15] LURE (Laboratoire pour l'Utilisation du Rayonnement Electromagnétique, Orsay, France), now replaced by SOLEIL (Source Optimisée de Lumière d'Energie Intermédiaire du LURE, St. Aubin, France).

[16] V. Pierron-Bohnes, I. Mirebeau, E. Balanzat, and M. C. Cadeville, J. Phys. F: Met. Phys. **14**, 197 (1984).

[17] G. R. Harp, D. Weller, T. A. Rabedeau, R. F. C. Farrow, and M. F. Toney, Phys. Rev. Lett. **71**, 2493 (1993).

[18] L. Bouzidi, V. Pierron-Bohnes, O. Haemmerle, C. Bouillet-Ulhaq, and M. C. Cadeville, Thin Solid Films **318**, 215 (1998).

[19] D. Halley, Y. Samson, A. Marty, C. Beigné, and B. Gilles, Surf. Sci. **481**, 25 (2001).

[20] M. C. Cadeville, V. Pierron-Bohnes, and J. M. Sanchez, J. Phys.: Condens. Matter **4**, 9053 (1992).

[21] M. Abes, M. V. Rastei, J. Venuat, A. Carvalho, S. Boukari, E. Beaurepaire, P. Panissod, A. Dinia, J. P. Bucher, and V. Pierron-Bohnes (unpublished).

[22] R. V. P. Montsouka, C. Goyhenex, G. Schmerber, C. Ulhaq-Bouillet, A. Derory, J. Faerber, J. Arabski, and V. Pierron-Bohnes, Phys. Rev. B **74**, 144409 (2006).